



CHORUS

This is the accepted manuscript made available via CHORUS. The article has been published as:

Local theory for Mott-Anderson localization

Sudeshna Sen, Hanna Terletska, Juana Moreno, N. S. Vidhyadhiraja, and Mark Jarrell

Phys. Rev. B **94**, 235104 — Published 2 December 2016

DOI: [10.1103/PhysRevB.94.235104](https://doi.org/10.1103/PhysRevB.94.235104)

A local theory for Mott-Anderson localization

Sudeshna Sen,¹ Hanna Terletska,² Juana Moreno,^{3,4} N. S. Vidhyadhiraja,^{1,*} and Mark Jarrell^{3,4,†}

¹*Theoretical Sciences Unit, Jawaharlal Nehru Centre for Advanced Scientific Research, Bangalore-560064, India*

²*Department of Physics, University of Michigan, Ann Arbor, Michigan 48109, USA*

³*Department of Physics & Astronomy, Louisiana State University, Baton Rouge, Louisiana 70803, USA*

⁴*Center for Computation & Technology, Louisiana State University, Baton Rouge, Louisiana 70803, USA*

The paramagnetic metallic phase of the Anderson-Hubbard model (AHM) is investigated using a non-perturbative local moment approach within the framework of dynamical mean field theory with a typical medium. Our focus is on the breakdown of the metallic phase near the metal-insulators transition as seen in the single-particle spectra, scattering rates and the associated distribution of Kondo scales. We demonstrate the emergence of a universal, underlying low energy scale, T_K^{peak} . This lies close to the peak of the distribution of Kondo scales obtained within the metallic phase of the paramagnetic AHM. Spectral dynamics for energies, $\omega \lesssim T_K^{peak}$ display Fermi liquid universality crossing over to an incoherent universal dynamics for $\omega \gg T_K^{peak}$ in the scaling regime. Such universal dynamics indicate that within a local theory the low to moderately low energy physics is governed by an effective, *disorder renormalised* Kondo screening.

1. INTRODUCTION

Disorder is ubiquitous in real materials, strongly influencing their properties¹⁻³. Another aspect of several condensed matter systems like the heavy fermions or transition metal oxides is the presence of strong electron-electron interactions^{4,5}. In particular, Coulomb correlations and disorder may individually drive a system towards a metal-insulator transition. While the Anderson metal-insulator transition⁶ is caused by quenched disorder, the Mott-Hubbard metal-insulator transition emerges from strong Coulomb repulsion⁵. The simultaneous presence of disorder (W) and interaction (U) effects is known to influence material properties in subtle ways. Over the last few decades, several experimental works on a range of systems^{1,7-14} have highlighted the importance of the interplay of disorder and interactions. The early theoretical studies of such systems¹⁵ mainly focused on the weak disorder limit, perturbing around Fermi liquid theory. It is now known that the subtle interplay of disorder and interactions may lead to non-Fermi liquid like responses in the thermodynamic quantities, as observed in several experiments⁸; therefore, one requires a non-perturbative framework that can deal with interactions and disorder on an equal footing.

One of the most intriguing aspects of strongly correlated electron systems is the appearance of low-energy scales¹⁶⁻¹⁸. For metals with strong electronic correlations a frequently observed scenario is the presence of long-lived quasi-particles representing a coherent Fermi liquid picture at the lowest temperatures (T) and energy scales. A universal low energy scale, T^* , lies at the heart of all strongly correlated electron systems that manifests in the universal transport properties of these materials¹⁸. Over the past few decades, the dynamical mean field theory (DMFT) has stood out as a very successful theoretical framework for understanding several aspects of the low energy physics of strongly correlated electron systems⁵. Since, in DMFT, any lattice-fermion model reduces to a

local quantum impurity model, the involvement of Kondo physics is inevitable. Thus, universal behavior due to the emergence of a universal low energy scale is generally attributed to the underlying Kondo effect. For example in the DMFT picture of the metallic phase of the Hubbard model^{5,19}, the Kondo effect leads to full quenching of the electron spin degrees of freedom resulting in a non-degenerate Fermi liquid ground state characterized by a low energy Fermi liquid scale. In the vicinity of the Mott transition, the strongly correlated metal is therefore characterized by a low-energy scale corresponding to the coherence temperature of a Fermi liquid^{5,19}.

The emergence of a single low energy/temperature scale may not be restricted to clean strongly-correlated electron systems, but has also been predicted in the context of diluted two-dimensional electron gases (2DEGs)²⁰. Phenomenological theories, based on experimental observations in 2DEGs^{7,21,22}, established a similarity between the metal-insulator transitions in such disordered systems and the conventional Mott-Hubbard metal-insulator transition. Studies in these directions are important for understanding the true driving force behind metal-insulator transitions observed in disordered interacting systems. A finite temperature study of the effects of disorder on the non-zero temperature Mott transition²³ also revealed the prevalence of a single parameter scaling of the distribution of quasi-particle weights in the vicinity of a disordered Mott transition.

A natural question that follows from these studies is whether such scaling with respect to a single low energy scale also manifests in the dynamics of the microscopic quantities like the single particle spectra or the disorder averaged scattering rate in a disordered interacting system at zero temperature. And if such universal dynamics exists, then how general is this observation across the $W - U$ phase diagram? The origin and evolution of such low energy scales with respect to W and/or U would then reflect upon the driving force behind the localization of the electrons.

The understanding of the behavior of the low en-

ergy scales in a strongly correlated system thus stand out as a key prerequisite irrespective of the presence or absence of disorder. Several theoretical frameworks have attempted to understand the interplay of disorder and strong correlations^{24–26}. However, the study of emergent low energy scales in the simultaneous presence of disorder and electron-electron interactions require non-perturbative frameworks. Studies using the framework of the DMFT have provided several insights in these directions. A computationally inexpensive approach involves the framework of DMFT and utilization of the ‘typical’ density of states (TDoS, ρ_{typ})^{27,28} for self-consistently obtaining the effectively local hybridizing medium, $\Gamma(\omega)$ ^{29–33}, in which the single impurities are embedded. This construction of the DMFT bath utilizing the $\rho_{typ}(\omega)$ is known as the TMT-DMFT framework³². The TDoS is most appropriately approximated as the geometric average of the local density of states (LDoS), $\langle \rho(\omega) \rangle_{geom} = \rho_{typ}(\omega) = \exp\langle \ln \rho_i(\omega) \rangle$ with $\rho_i(\omega)$ being the local density of states. Another way of representing this is $\rho_{typ} = \exp \int dV_i P(V_i) \ln \rho_i(\omega)$, where V_i represents the bare random potential and $P(V_i)$, the probability distribution followed by these bare site energies. While, $\rho_{typ}(0)$ is critical at the Anderson transition^{34,35}, the average density of states (ADoS) given by $\rho_{arith}(\omega) = \int dV_i P(V_i) \rho_i(\omega)$ is not critical. The TDoS behaves like an order parameter for the metal-insulator transition originating in the metallic phase; in the insulating phase it is trivially zero at all frequencies. Thus, in principle the TMT framework is designed to capture the physics of the metal-insulator transition approaching from the metallic phase.

The TMT-DMFT method was first applied to the Anderson-Hubbard model by Byczuk *et al.*²⁹ who explored the $W - U$ paramagnetic phase diagram using numerical renormalization group (NRG) as the impurity solver. Three distinct phases were identified namely, a correlated metallic phase, a Mott insulating phase and an Anderson insulating phase. Additionally, a coexistent regime of the metal-Mott insulating phase was reported. The Mott and Anderson insulator phases were found to be continuously connected. The characterization of these phases were based on the behavior of the band center of the TDoS ($\rho_{typ}(0)$) and the ADoS ($\rho_{arith}(0)$). The metallic phase featured a non-zero $\rho_{typ}(0)$ and $\rho_{arith}(0)$. For weak to moderate W , a sharp transition from the metallic to a gapped insulating phase was observed where both $\rho_{typ}(0) = 0$ and $\rho_{arith}(0) = 0$. This metal-insulator transition was similar in characteristics with the conventional single band Hubbard model and hence this insulating phase was termed as the Mott insulator. Moreover, the density of states in this phase featured prominent Hubbard subbands. Additionally a metal-Mott insulator coexistence regime similar to the p-h symmetric single-band Hubbard model was identified in the $W-U$ plane that terminated at a single W . The Anderson insulator was characterized as a phase that featured $\rho_{typ}(0) = 0$ and $\rho_{arith}(0) \neq 0$. Additionally, the Hubbard bands were

broad and diffused.

Although, the NRG is highly efficient in capturing the Kondo effect, the distribution of Kondo scales, a natural occurrence in interacting disordered systems, was not explored in Ref. 29. Thus the role of the local Kondo scales could not be deduced from the above calculation. Such a direction was however explored using slave-boson mean-field theory calculations³¹, highlighting the role of the local quasi-particle weights, Z_i , that may also serve as an order parameter for the localization physics in the Anderson-Hubbard model. Close to the disorder driven metal-insulator transition at $U/W < 1$ a *two fluid* picture was proposed. Through TMT-DMFT calculations they proposed a spatially inhomogeneous picture where in certain regions there existed Mott fluid droplets with $Z_i \rightarrow 0$ and at other regions $Z_i \rightarrow 1$ representing Anderson localized particles. Irrespective of the spatially inhomogeneous picture, one would expect a metal-insulator transition to occur at a critical disorder strength, W_c , when the U is fixed, and this would coincide with the vanishing of the impurity hybridization obtained from the TDoS. A conventional Mott-like picture was proposed to prevail for the U driven metal-insulator transition at sufficiently small disorder strengths. A similar line of reasoning based on the behavior of the impurity hybridization would lead us to expect that the Mott upper critical interaction, U_{c2} , would coincide with the vanishing of the impurity hybridization obtained from the TDoS.

However, it is also well known that slave-boson based solvers fail to account for inelastic scattering and thus fail to predict the correct lineshape of spectral functions and scattering rates^{36,37}. Moreover, the physics at low energies, may be highly affected by the physics at higher energy scales. Thus, in order to have a precise understanding of the spectral/dynamical properties in a correlated system, we require all energy scales and interaction strengths, from weak to strong coupling, to be handled within a unified theoretical framework. In this work we revisit the metallic phase of the Anderson-Hubbard model using the local moment approach (LMA)³⁸ as an impurity solver within the TMT-DMFT. The LMA has been successfully applied for several impurity^{38–40} and lattice models^{16,41–43} (within DMFT). The LMA is known to capture the Kondo effect correctly while also capturing the correct lineshape of the spectral functions. With this set up we look into the evolution of the distribution of Kondo scales as a function of W and U . Additionally, we explore the scattering dynamics within the current non-perturbative local framework, and identify universal dynamics and scaling similar to the clean interacting scenario. It should be noted that all the calculations presented in this work pertain to the metallic phase and an exploration of the insulating phases is beyond the scope of the current work. These results are therefore relevant in the context of the breakdown of the metallic phase towards Mott or Anderson localization.

2. MODEL

The Anderson-Hubbard model is considered as a paradigmatic model for looking into the interplay of strong electron interactions and disorder. It is given by,

$$\hat{H} = - \sum_{\langle ij \rangle, \sigma} t_{ij} \left(c_{i\sigma}^\dagger c_{j\sigma} + \text{H.c.} \right) + \sum_{i, \sigma} (V_i - \mu) \hat{n}_{i\sigma} + U \sum_i \hat{n}_{i\uparrow} \hat{n}_{i\downarrow}, \quad (1)$$

where, $c_{i\sigma}^\dagger$ ($c_{i\sigma}$) is the fermionic creation (annihilation) operator for an electron with spin σ at site i , and $\hat{n}_{i\sigma} = c_{i\sigma}^\dagger c_{i\sigma}$, t_{ij} is the nearest neighbour site hopping amplitude considered to be constant in this work, U is the onsite Coulomb interaction energy. The lattice is represented by a three-dimensional cubic DoS with full bandwidth, $D = 3$. The random local potential V_i follows a "box" distribution $P(V_i)$ such that $P(V_i) = \frac{1}{2W} \Theta(W - |V_i|)$, where $\Theta(x)$ is the Heaviside step function. A global particle-hole symmetry is imposed by $\mu = U/2$. At $W = 0$, this model reduces to the particle-hole (p-h) symmetric single-band Hubbard model, which displays a first order Mott transition at zero temperature, $T = 0$, as a function of U . On approaching this transition from the Fermi liquid (FL) side, the Kondo scale, T_K^0 vanishes at a critical point, U_{c2} , marking the transition to the Mott insulating state. On approaching from the Mott insulating side, the Mott gap vanishes at a critical point, U_{c1} , where, $U_{c1} < U_{c2}$. This scenario in the $W = 0$ case motivates us to look at the regimes, $U < U_{c2}$ and $U > U_{c2}$ distinctly. For a three-dimensional simple cubic DoS, within the LMA, we have found out that the Mott MIT occurs at $U_{c2}/D \sim 0.8$ which corresponds to $U_{c2} \approx 2.3$, the bandwidth (D) being equal to 3. This result compares well with the value predicted by NRG calculations ($\sim 1.1D$)⁴⁴.

For treating non-zero disorder in the presence of interactions (Eq. (1)) we employ the TMT-DMFT framework where we map the disordered lattice model on to an ensemble of single impurity Anderson models, each embedded in a self-consistently determined effective medium, $\Gamma(\omega)$, which is obtained from $\rho_{typ}(\omega)$, as described in Appendix B. The reader is also referred to several previous works^{29-31,33,34} for the details of the formalism. In Appendix A and B we also describe the implementation of the LMA within the TMT-DMFT framework. We typically solve for $\sim 10^5$ disorder realizations each of which involves the calculation of the local interaction self-energy, $\Sigma_i(\omega)$.

3. RESULTS AND DISCUSSIONS

In the absence of interactions, Eq. (1) reduces to the Anderson model of non-interacting electrons⁶. Here, the metal to insulator transition is not characterized by the

vanishing of the DoS. Instead, the hybridization paths get canceled accompanied by weak localization of the wave functions due to coherent backscattering from impurities or exponential localization of the wave functions in deep-trapped states^{2,18,45}. As a result, the electrons occupying such exponentially localized states are confined to limited regions in the space and cannot contribute to the transport. As the disorder potential, W , is increased, more and more regions in space become exponentially localized and the system undergoes a metal-insulator transition as a function of W . At the Anderson localization transition the average DoS given by, $\rho_{arith}(\omega) = \int dV_i P(V_i) \rho_i(\omega)$, with $\rho_i(\omega)$ being the LDoS, is not critical. However, the geometrical mean of the LDoS, $\rho_{typ} = \exp \int dV_i P(V_i) \ln \rho_i(\omega)$, better approximates the critical nature of the Anderson localization transition. The local TMT framework adopted here reproduces some of the expected features of the Anderson localization transition, but underestimates the critical disorder strength, W_c ³⁵. Although by construction the local TMT framework is able to describe qualitatively the effects of strong localization due to disorder, all non-local coherent backscattering effects are lost. The localization mechanism *explicitly* contained within the TMT is essentially the physics due to deep-trapped states where the states initially above and below the bare band-edge become localized in deeply trapped states^{2,45,46}. This effect is subsequently fed back into the hybridizing medium so that the band center also localizes. Within TMT, the band edge of $\rho_{typ}(\omega)$ then monotonically moves towards the band center such that at the critical disorder strength even states at the band center are exponentially localized.

Perturbative studies on the weakly interacting disordered electron gas dates back to the seminal work of Altshuler and Aronov²⁴. Later extensions include the two-loop large- N reormalization group analysis of Punnoose and Finkelstein²⁵, that could describe a metal-insulator transition in a two-dimensional electron gas. However, in disordered interacting systems there also exists a number of relevant phenomena that are beyond the reach of perturbative methods. For example, the work by Milanović, Sachdev and Bhatt⁴⁷ and later by Bhatt and Fisher⁴⁸ showed the importance of disorder in describing the instability of a disordered, interacting Fermi liquid towards the formation of local moments. The treatment of interactions within the non-perturbative framework of DMFT⁵ can naturally incorporate the tendency towards the formation of local moments³¹. In this work, we revisit the paramagnetic phase of the AHM and try to elucidate the mechanism that could lead to the formation of such local moments in a disordered, interacting system. In particular, we look into the single particle quantities across a broad range of U and W parameters, putting particular emphasis on the scattering rate and the evolution of the distribution of Kondo scales with respect to U and W .

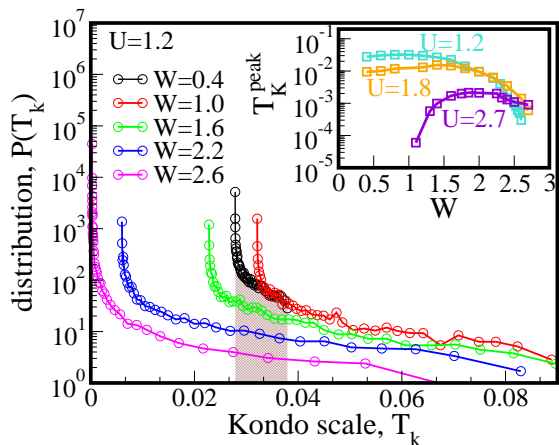


FIG. 1. **Distribution of Kondo scales:** In the main panel, the evolution of the T_K distribution as a function of W for $U = 1.2$ is shown on a linear-log scale. The distributions are peaked and (sharply) bounded from below by T_K^{peak} , the scale associated with the respective particle-hole symmetric limit of the effective impurity problem embedded in the *typical* medium. The shaded region highlights the narrow range of T_K 's spanned by small W in contrast to the higher T_K long tails spanned by larger W 's. (inset) T_K^{peak} is plotted as a function of W for $U = 1.2, 1.8, 2.7$. While, $U = 1.2, 1.8$ correspond to $U < U_{c2}$, $U = 2.7 > U_{c2}$. Hence, in the $W = 0$ limit $U = 1.2$ and $U = 1.8$ correspond to Fermi liquids with $T_K^0 = T_K^{peak} \approx 0.025$ and 0.007 , respectively. On the other hand, $U = 2.7$ corresponds to a Mott insulator with $T_K^0 = T_K^{peak} = 0$.

3.1. Distribution of Kondo scales:

It is well known that the metallic DoS of the particle-hole symmetric single-band Hubbard model exhibits a three peak structure, with a well defined Abrikosov-Suhl resonance centered around the Fermi energy, that signifies the low-energy quasiparticle coherence present in the system, symptomatic of an underlying coherence scale, T_K^0 ⁵. The full width at half maximum of this resonance is one measure of the low energy Kondo coherence scale, T_K^0 , present in the Fermi liquid. The local quasi-particle weight, $Z = \left(1 - \frac{\partial \text{Re}\Sigma(\omega)}{\partial \omega}\right)^{-1}$ provides another measurement of this energy scale. Above this coherence scale, physical properties are dominated by incoherent electron-electron scattering effects and Fermi liquid theory loses its validity although, recent state-of-art DMFT calculations indicate a *resilient quasi-particle* regime before the system crosses over to a bad metal regime⁴⁹. In the presence of disorder the translational invariance is broken, so the screening of the local moments by mobile electrons should be spatially non-uniform. While some sites may be strongly hybridized with the local medium, others may be weakly hybridized. For sites that are weakly hybridized with the local surroundings charge fluctuations are suppressed, thus representing a reduced screening in comparison to the sites that strongly hybridize with the

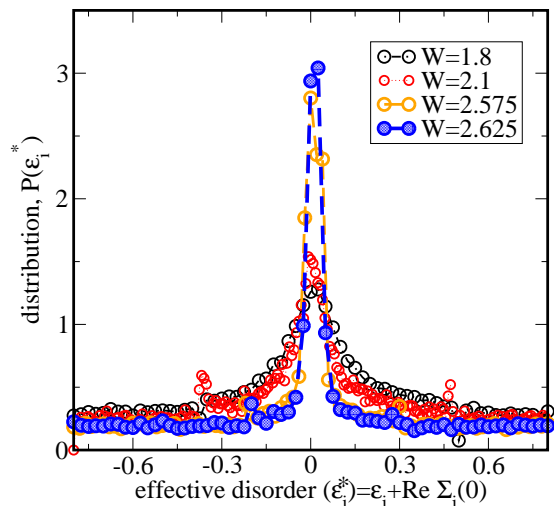


FIG. 2. **Distribution of the renormalized site energy,** $\epsilon_i^* = \epsilon_i + \text{Re}\Sigma_i(0)$, with $\epsilon_i = V_i - U/2$, plotted for $U = 1.2$ and $W = 1.8, 2.1, 2.575, 2.625$. A pronounced weight is observed around $\epsilon_i^* = 0$ that represents the particle-hole symmetric limit. The initially broad peak becomes narrower and grows in intensity as W is increased. Such an evolution of ϵ_i^* as a function of increasing W indicates that a majority of sites tend to attain a T_K close to that of the particle-hole symmetric limit. This can be correlated with the skewed nature of $P(T_K)$ in Fig. 1 as W is increased. Note that the entire range is not shown.

surrounding medium. Therefore, in a strongly correlated disordered system, the coherence scale is a random quantity with an associated distribution.

Within the TMT-DMFT implementation we solve an ensemble of impurity problems embedded in an effective disorder averaged medium. We use the LMA as our impurity solver. The LMA is designed to capture the dynamical spin flip scattering processes encountered by an \uparrow / \downarrow spin occupied impurity. These processes lie at the heart of the physics associated with the Kondo effect⁵⁰, and their energy scale is on the order of the Kondo scale. The LMA can capture such extremely low energy scales efficiently. Within the LMA, a measure of the Kondo scale is provided by the position of the resonance in the transverse spin polarization propagator⁵⁰. We therefore end up with a self-consistently determined distribution of such spin-flip scattering energy scales that represent the energies associated with the Kondo screening of the impurities by the disorder averaged effective non-interacting host.

In Fig. 1 we show the distributions of Kondo scales, T_K , for various disorder strengths, W , at a fixed $U = 1.2$. The local nature of the framework renders the distributions to be peaked and bounded from below (also observed in earlier works at non-zero temperature²³ and square lattice⁵¹). This peak, T_K^{peak} , is associated with the particle-hole (p-h) symmetric limit of the effective impurity problem embedded in the disorder averaged medium that is also p-h symmetric and is identical for all such

single-impurity sites. Due to the local nature of the solution, the effective Kondo screening experienced by any impurity moment could thus be only dependent on the V_i of the respective impurity. Therefore sites which are at or close to the p-h symmetric limit will experience the least Kondo screening and hence will have the lowest T_K . The shaded region in Fig. 1 demonstrates the narrow area under the curves corresponding to the low disorder limit of $W = 0.4$ for $U = 1.2$, in contrast to the long tails in the distributions corresponding to the higher values of W . The initial effect of increasing W is to screen the effects

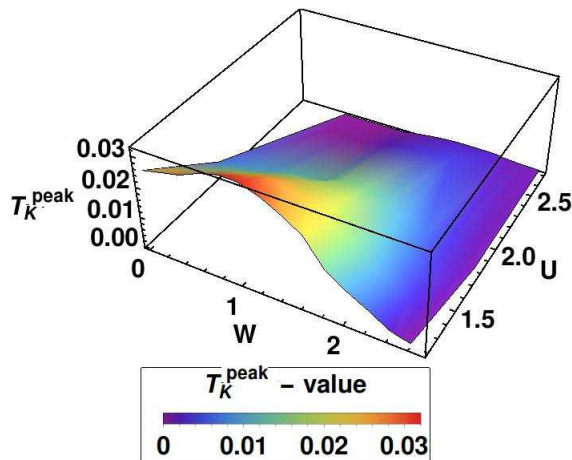


FIG. 3. A schematic of the surface formed by the T_K^{peak} as a function of U and W .

of U even at the lowest energy scales, such that T_K^{peak} is pushed to higher values; subsequently, with increasing W , T_K^{peak} decreases monotonically, signifying the onset of disorder induced scattering cooperating with interaction driven scattering in the low frequency region, and tending to localize the system.

In the inset of Fig.1 we plot T_K^{peak} as a function of W for different interaction strengths, U . When $W = 0$, the systems with $U = 1.2$ and 1.8 are Fermi liquids with Kondo scales $T_K^0 = T_K^{peak} \approx 0.025$ and 0.007 , respectively. For $U = 2.7$, the system is a Mott insulator with $T_K^0 = T_K^{peak} = 0$. As shown in the inset of Fig.1, for $U = 2.7$ ($U > U_{c2}$), the T_K^{peak} evolves from being zero at low $W \ll U$, and then at $W = W_{c1}$ a non-zero T_K^{peak} emerges that subsequently increases with increasing disorder signifying a regime where disorder screens the effects of strong interactions. This initial screening of electron-electron interactions due to disorder is true even for smaller $U = 1.2$ or $U = 1.8$ ($U < U_{c2}$) as discussed earlier. Subsequently, $T_K^{peak} \rightarrow 0$ as W is increased, an observation that holds true for both $U = 1.2$ and $U = 1.8$.

Particular insight about the respective behavior of $P(T_K)$ may be obtained by looking at the evolution of the *effective* site potential energy (ϵ_i^*) as a function of increasing W . In Fig. 2 we show the distribution of the disorder renormalised site energy, $P(\epsilon_i^*)$, for $W = 1.8, 2.1, 2.575, 2.625$ at $U = 1.2$, with

$\epsilon_i^* = V_i - U/2 + \text{Re}\Sigma_i(0)$. The distribution is marked by a peak around $\epsilon_i^* = 0$, indicating that a majority of sites tend to attain a disorder renormalized site potential energy close to the p-h symmetric limit. This explains why the T_K^{peak} is determined by the Kondo scales corresponding to the sites that are at or close to half-filling. This peak is initially broad for a relatively low W ($W = 1.8$) and becomes sharper as the W is increased. This shows that as the disorder is increased more number of sites experience a reduced Kondo screening. In other words, for stronger W 's, the distribution of Kondo scales become more and more skewed such that even sites that are quite far away from half filling may experience a reduced Kondo screening resulting in a Kondo energy scale close to that corresponding to the p-h symmetric limit.

It is to be noted that such a behavior of $P(\epsilon_i^*)$ has been shown to exist close to an *interaction* driven transition at a fixed W ^{52,53}, where such a behavior of $P(\epsilon_i^*)$ has been dubbed as *perfect disorder screening*. In other words similar observations were shown to be prevalent close to the metal-Mott insulator phase boundary of the symmetric, paramagnetic AHM^{52,53}. In this work, we show that this behavior of $P(\epsilon_i^*)$ and $P(T_K)$ is generic to a broader parameter regime. These observations are not just restricted to U driven metal-insulator transition at low W , but applies to W driven transitions also even if the bare interaction strength is small. The physical picture underlying the above observation is the following: for strong disorder potential, as we approach a disorder driven metal-insulator transition, the $\Gamma_{typ}(0)$ between any site and its host becomes sufficiently small such that the ratio, $U/\pi\text{Im}(\Gamma_{typ}(0)) \gg 1$, and these sites with $\epsilon_i^* \sim 0$ experience stronger interaction effects, pushing T_K^{peak} towards zero, even though the bare interaction strength is small. In Fig. 3 we summarize the above analysis by representing the surface of T_K^{peak} scales as a function of both U and W . Since T_K^{peak} represents the most probable value of the underlying Kondo scale, we now ask the question whether this can be related to the scattering dynamics of the system close to the metal-insulator transitions observed in the AHM. In the following section we therefore explore the imaginary part of the disorder averaged self-energy, $-\text{Im}\Sigma_{ave}(\omega)$.

3.2. Scattering dynamics

In a strongly correlated system the imaginary part of the interaction self-energy, $-\text{Im}\Sigma(\omega)$, relates to the scattering rate. Thus the $-\text{Im}\Sigma(\omega)$ is a mirror of the underlying scattering dynamics present. In a disordered interacting system we need to look at the average self-energy, $-\text{Im}\Sigma_{ave}(\omega)$, obtained from the arithmetically averaged Green's function, $\langle G(\omega) \rangle_{arith}$, where $\langle \dots \rangle_{arith}$ denotes arithmetic averaging with respect to $P(V_i)$. It is this average quantity that represents the physical Green's function of the system. The quantity, $\langle G(\omega) \rangle_{arith}$ may

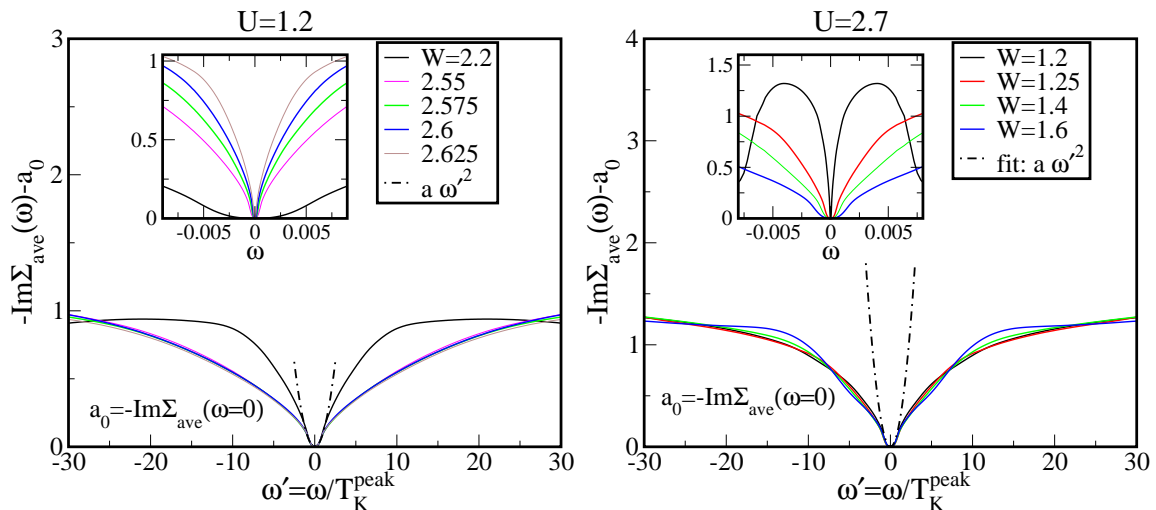


FIG. 4. **Universal scaling of $-\text{Im}\Sigma_{ave}(\omega)$:** (Left main panel) The $-\text{Im}\Sigma_{ave}(\omega)$ with the static part ($a_0 = -\text{Im}\Sigma_{ave}(0)$) subtracted is plotted for $U = 1.2$, on an energy scale, ω' , with the bare frequency, ω rescaled by T_K^{peak} that has been obtained from the respective $P(T_K)$ plots. (Left inset) The same sets of data are plotted on a bare energy scale, ω . (Right main panel) The $-\text{Im}\Sigma_{ave}(\omega)$ with the static part ($a_0 = -\text{Im}\Sigma_{ave}(0)$) subtracted is plotted for $U = 2.7$ on the rescaled energy scale, ω' . (Right inset) The same sets of data are plotted on a bare energy scale.

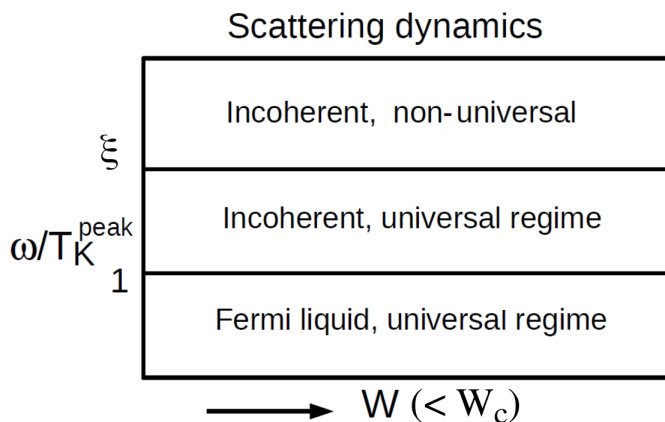


FIG. 5. A schematic demonstrating the self-energy scattering dynamics corresponding to different energy regimes as a function of disorder, W within the metallic phase. It should be noted that the quantity ξ separating the ‘incoherent universal’ and the ‘incoherent non-universal’ regimes is just symptomatic of the proximity to the metal-insulator transition. In strong coupling as $W \rightarrow W_c$, where W_c is the critical disorder strength for the metal-insulator transition when approached from the metallic side, $\xi \rightarrow \infty$ in the scaling regime.

be obtained from the Hilbert transform of $\rho_{arith}(\omega)$, given by, $\langle G(\omega) \rangle_{arith} = \int \frac{\rho_{arith}(\omega') d\omega'}{\omega - \omega'}$. Accordingly, the average self-energy, that represents the scattering dynamics, is obtained from the Dyson’s equation given by $\Sigma_{ave}(\omega) = \mathcal{G}(\omega)^{-1} - \langle G(\omega) \rangle_{arith}^{-1}$. The host Green’s function $\mathcal{G}(\omega)$ embodies the *typical* nature of the disorder-averaged medium.

In a clean Fermi liquid, the $-\text{Im}\Sigma_{ave}(\omega) = -\text{Im}\Sigma(\omega) \sim$

$|\omega|^2$ for $\omega < T_K^0$ (where T_K^0 is the lattice-coherence scale or the Kondo scale in a clean lattice). With this background we look at the low frequency region of $-\text{Im}\Sigma_{ave}(\omega)$. In Fig. 4, we subtract the static contribution of the impurity scattering, $a_0 = -\text{Im}\Sigma_{ave}(0)$ and plot the quantity, $-\text{Im}\Sigma_{ave}(\omega) - a_0$ for various disorder strengths at fixed interaction strengths, $U = 1.2$ (left panel) $U = 2.7$ (right panel). The parameters presented are close to the disorder driven metal-insulator transition boundary. In the main panels we plot this quantity on a frequency rescaled, $\omega' = \omega/T_K^{peak}$ axis, relating T_K^{peak} to the inverse scattering rate of the particles. The insets to these figures show the low frequency part of the self-energy spectrum, $-\text{Im}\Sigma_{ave}(\omega) - a_0$, on an absolute scale, i.e. vs. ω . In either case ($U = 1.2$ or $U = 2.7$) of Fig. 4 the self-energy spectrum for various W ’s look quite distinct on the bare energy scale being dependent on the disorder strength, W . These plots also reflect upon the diminution of the *effective* Kondo scale as W is increased, thus relating to Fig. 1. In contrast to the insets of Fig. 4, the main panels of Fig. 4 illustrate the self-energy spectrum on a rescaled axis, with the rescaled frequency, $\omega' = \omega/T_K^{peak}$. It is also observed that the low energy spectral dynamics of $-\text{Im}\Sigma_{ave}(\omega) - a_0 \sim \omega'^2$ for $\omega' < 1$. At higher energy scales, a clear departure from $\sim \omega'^2$ is evident as anticipated. A universal scaling collapse of the single-particle self-energy, with respect to T_K^{peak} is observed reminiscent of the conventional correlated lattice scenario^{19,54}. The clear collapse due to this rescaling suggests that, within a local theory, even in presence of a random potential, an energy scale $\sim T_K^{peak}$ serves as a Fermi liquid scale, just as in the clean case. Moreover, as seen from the main panel of Fig. 4, although the coherent Fermi liquid scattering

regime is restricted for $\omega' \leq 1$, a universal scattering dynamics is significantly observed until much higher energy scales. In other words, this signifies that within a local theory for interacting disordered systems, the quasi-particle excitations are in fact determined by a disorder renormalized single impurity Kondo scale, T_K^{peak} . Let us now comment on the parameter regime where this collapse is most significantly observed. The scaling collapse for $U = 1.2$ holds true for higher disorders and very close to the transition where the T_K^{peak} itself is exponentially small. Note that the values of $W = 2.575, 2.6, 2.625$ in Fig. 4 correspond to very small scales in Fig. 1. So, in Fig. 4(left panel) representing $U = 1.2$, the W 's represent values close to the metal to a disorder driven Mott-Anderson insulator transition. A similar scenario is observed for $U = 2.7$, as shown in the right panel of Fig. 4. If we now locate $W = 1.2, 1.25, 1.4$ in Fig. 1 (violet curve), these values would approximately correspond to $T_K^{peak} \sim 0.00009, 0.0005, 0.001$ respectively, and would thus represent W 's close to a metal-insulator transition resembling a clean Mott transition. Note that according to Ref. 29, at the critical disorder strength where this metal-insulator transition would occur the $\rho_{typ}(0), \rho_{arith}(0)$ would vanish simultaneously, 'on the spot'. In Ref. 29, the insulating phase resulting from this transition was termed as the disordered Mott insulator phase. In accordance with the observations of Ref. 31, we also speculate that the T_K^{peak} would continuously vanish to zero at the critical W . So, as observed in Fig. 4, universal scaling, until $\omega \gg T_K^{peak}$ is observed from $W = 1.2$ and $W = 1.25$, representing parameters very close to the *disordered Mott transition*. Note that since we could not reach such low energy scales for the metal to Mott-Anderson insulator transition at higher W for $U = 2.7$, demonstrating such a scenario in this regime was beyond the scope of the current work.

We note in passing, that such a universal scaling collapse scenario could already be anticipated from Fig. 2 where we demonstrated the evolution of the distribution of the renormalised site energies, ϵ_i^* as a function of increasing disorder. As W is increased in presence of a fixed U , the pronounced tendency of an appreciable number of sites to acquire a renormalised site potential, $\epsilon_i^* = 0$, already reflect upon the possible emergence of a universal low energy scale close to the disorder driven metal-insulator transition. This in turn manifests as a universal scaling collapse in the spectral dynamics of $-\text{Im}\Sigma_{ave}(\omega) - a_0$. This *renormalized* single-particle dynamics is summarized in Fig. 5 as a schematic. Such universal physics determined by a single energy scale, even in the presence of strong disorder, suggests that the local effect of disorder is to only renormalize the onsite interaction between the electrons, such that the underlying low energy quasiparticle excitations are still determined by Fermi liquid dynamics, similar to a conventional Mott transition scenario. This is possibly a consequence of the underlying scattering mechanism due to deep-trapped states prevalent within a local theory

and its resulting feedback to the low energy sector of the (local) hybridizing medium. It is worth mentioning that a similar universal scaling scenario of the single particle density of states was hinted at in an earlier study by Aguiar *et al.* in Ref. 30. They considered an ensemble of single impurity Anderson models embedded in a model bath. The model bath was manually chosen, and the *typical* nature of the hybridization function was parametrized in order to mimic a disorder driven metal-insulator transition. In this work we elucidate and demonstrate a universal scaling picture of scattering dynamics within a self-consistent scheme, where the *typical* medium is determined self-consistently and depends on the amount of disorder present.

3.3. Density of states

The arithmetically averaged DoS (ADoS) is defined as, $\rho_{arith}(\omega) = \int P(V_i)\rho_i(\omega) dV_i$, where, $\rho_i(\omega)$ is the local DoS (LDoS). The typical DoS is obtained via geometric averaging of the LDoS and is defined as, $\rho_{typ}(\omega) = \exp \int P(V_i) \ln \rho_i(\omega) dV_i$. As mentioned earlier, $P(V_i)$ represents the distribution followed by the random site potential energies, that in this paper is chosen to be a box distribution. In Fig. 6(a), we plot the arithmetically averaged DoS (ADoS) and the typical DoS (TDoS) for various $W = 0.4, 1.2, 2.5$ at a fixed interaction strength $U = 1.2 < U_{c2}$. In agreement with the $U = 0$ scenario, when the disorder, W , is small, both the ADoS and the TDoS produce almost the same density of states. With increasing disorder, the TDoS gets suppressed over all energy scales (note that this is not spectral weight transfer, as the TDoS is not normalized). As seen from Fig. 6(a) there exists remnants of the $W = 0$ limit Kondo resonance centered around $\omega = 0$. With increasing disorder, this resonance initially broadens but then progressively narrows down. In Fig. 6(b), we plot the same as above but for $U = 2.7 > U_{c2}$ that represents a Mott insulator in the $W = 0$ limit of the p-h symmetric AHM. The introduction of randomness allows for local charge fluctuations that in turn leads to delocalization of the otherwise localized moments, beyond a certain critical disorder strength, W_{c1} . This picture is in agreement with the NRG calculations of Ref. 29. This naturally manifests as the emergence of a finite density of states at the Fermi level ($\omega = 0$). In other words, a sharp Kondo resonance reappears in the middle of a prominent gap, with the inclusion of a finite amount of disorder, W_{c1} ; this gap reminds us of the Mott insulating gap in the $W = 0$ limit. Based on the spectral fingerprints, we may speculate the following: if we start from $W = 1.1$ at $U = 2.7$ and decrease W we should expect a metal-insulator transition at W_{c1} . This transition is similar to the Mott metal-insulator transition obtained in the conventional single band Hubbard model. This should be reflected as the narrowing of $(P(T_K))$ (not shown here for $U = 2.7$) and an associated decrease in T_K^{peak} as W is

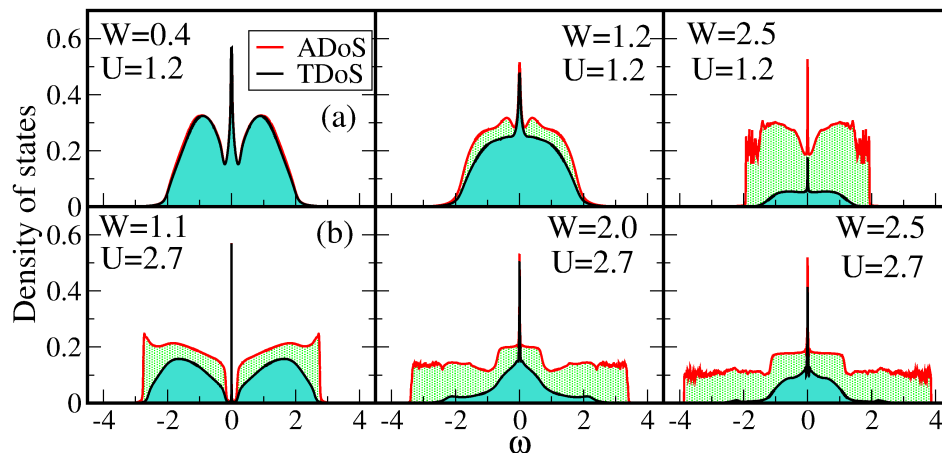


FIG. 6. **Evolution of the density of states:** The arithmetic mean of the density of states (DoS) also known as the average DoS (ADoS) (solid red line, green shaded region) and the geometric mean of the DoS also known as the typical DoS (TDoS) (solid black line, turquoise shaded region) at various W for (a) $U = 1.2$, (b) $U = 2.7$. Similar to the $U = 0$ scenario, when the disorder, W , is small, both the ADoS and the TDoS produce almost the same density of states and as W increases the TDoS gets suppressed over all energy scales.

pushed towards W_{c1} . The latter is illustrated in the inset of Fig. 1. For both Fig. 6(a) and Fig. 6(b), the high energy Hubbard bands broaden and acquire reduced spectral intensities. This broadening that is also manifested in the self-consistently determined hybridization function (not shown here) highlight the fact that presence of disorder introduces additional scattering pathways. In the context of DMFT, this increases the rate at which these high energy electrons hop off from the impurity site into the embedding host, thus reducing its lifetime and hence broadening the spectra at such energy scales.

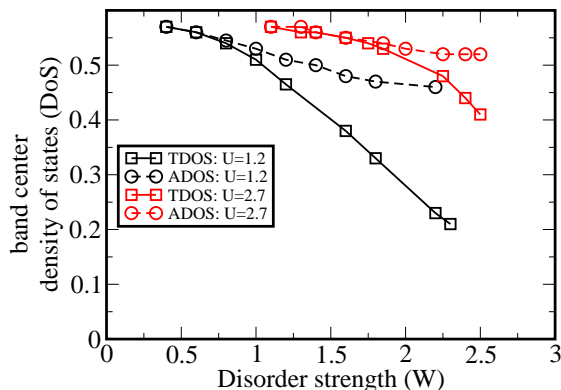


FIG. 7. Comparison of the band center ($\omega = 0$) value of the TDoS and the ADoS as a function of W .

To conclude this section, we compare the decay of the $\rho_{typ}(0)$ and the $\rho_{arith}(0)$ for the two regimes of interaction discussed above, namely, $U = 1.2 (< U_{c2})$ and $U = 2.7 (> U_{c2})$. From Fig. 7, $\rho_{typ}(0)$ appears to be monotonically vanishing as W is increased while $\rho_{arith}(0)$ appears to saturate. If the metal-insulator transition encountered at large W is continuous, as expected for small values of U , then these results suggest that the $\rho_{arith}(0)$

remains finite even in the insulating phase such that the Anderson-Mott insulator phase is gapless²⁹. A true characterization of the phases would require numerical simulations very close to the metal-insulator transitions. The numerical calculations become very unstable as one approaches this limit and hence is beyond the scope of the current work. Nevertheless, based on the above discussion, we demonstrate a qualitative picture of the different phase boundaries in Fig. 8. The different boundaries are all based on the approach from the metallic side. The phase boundary between the metal and the Mott-Anderson insulator phase is obtained by extrapolating $\rho_{typ}(0)$ to zero and the metal-Mott insulator phase boundary is obtained by extrapolating $T_K^{peak}(0)$ to zero. It is worth noting that for $U = 2.7$, both T_K^{peak} (as shown in the inset of Fig. 1) and $\rho_{typ}(0)$ (as shown in the inset of Fig. 7) appear to decay much more gradually than those for $U = 1.2$. In Ref. 29, indeed a slow decay of $\rho_{typ}(0)$ was attributed to the observation of a ‘crossover’ regime, where a sharp metal-insulator transition could not be rigorously identified. They reported it as a smooth crossover from the metallic to the insulating phase. It is true that, for $U = 2.7$ ($U > U_{c2}$) our observations are similar, in terms of the slow decay of $\rho_{typ}(0)$; however, we believe prediction of a ‘crossover’ instead of a ‘sharp transition’ is difficult within the current implementation, unless we probe deeper into the metallic regime and explore the insulating phase as well. It should also be noted that the presence of a preformed gap in the density of states shown in Fig. 6 in the regime where $W \ll U$ and $U > U_{c2}$ perhaps indicate the presence of a first-order Mott transition in this regime. While we obtain a similar trend as that obtained by Byczuk *et al.* in Ref. 29 or by Aguiar *et al.* in Ref. 31, since our current formulation lacks the ability of approach from the insulating side we cannot make any assertive statement about the metal-Mott insulator

coexistence regime or the crossover regime observed in Ref. 29.

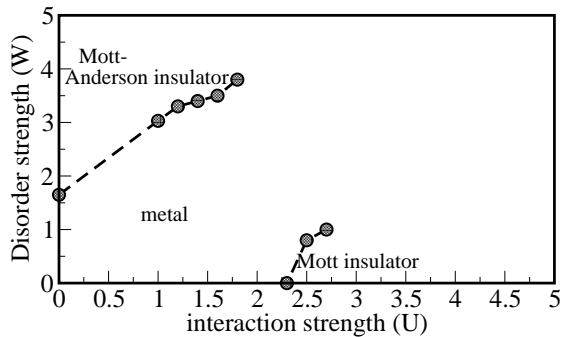


FIG. 8. A qualitative phase diagram of the Anderson-Hubbard model, within the TMT-DMFT framework. We approach from the metallic side and identify the phase boundary based on the behaviour of the peak T_K^{peak} of the distribution of Kondo scales and/or the band center value of the typical density of states, $\rho_{typ}(0)$. For example, both $\rho_{typ}(0) \rightarrow 0$ and $T_K^{peak} \rightarrow 0$ as the Mott-Anderson phase boundary is approached from the metallic side. On the other hand only $T_K^{peak} \rightarrow 0$ as the Mott phase boundary is approached from the metallic side.

4. CONCLUSIONS

We employed the dynamical mean field theory framework with a typical medium, to look into the interplay of disorder and strong correlations in the paramagnetic metallic phase of the particle-hole symmetric Anderson-Hubbard model using the local moment approach. Particularly, we explored the single particle dynamics by analyzing the disorder averaged self-energy and identified the existence of a universal ‘Kondo’ scale within such a local theoretical framework that considers the strong correlation physics in presence of disorder scattering only due to deep trapped states. Additionally, we showed that this scale could be represented by the peak (T_K^{peak}) in the distribution function of the Kondo scales. Moreover, the universal regime is shown to exist up to significantly high energies, although a strict Fermi liquid scattering dynamics holds true for $\omega \lesssim T_K^{peak}$. While such universal dynamics similar to that observed in the strong coupling limit of the conventional single-band Hubbard model^{19,54} is anticipated in the low disorder regime²³, the same is surprising in the proximity of an Anderson-Mott transition, where the disorder is much stronger in comparison to the interaction. But then, such an observation highlights the incipient disorder renormalised Kondo screening of the local moments to be the dominant mechanism determining the low energy physics of the system.

As mentioned before, within the local framework of the dynamical mean field theory in combination within the typical medium theory, the Anderson-Hubbard model is mapped onto an ensemble of impurity problems, where

the host for the impurities is determined by the typical density of states. The tendency of an impurity site to form a local moment is governed by the impurity-host hybridization function that is determined by the typical impurity density of states. Thus the low energy physics will be determined by the peak of the distribution of the density of states and reinforced by this self consistency since all the sites see the same hybridization function. In this case, these sites are the ones with the lowest Kondo scale, which are at the peak of the distribution. They are the ones closest to Mott character. The inhibition of the low energy hybridization function would be felt by all the impurities leading to a pronounced tendency towards forming local moments.

Since the disorder, especially near an Anderson localization transition, strongly suppresses the hybridization to the impurity, our observations highlight that in a disordered interacting system, Anderson and Mott mechanism of localization may not be disentangled. It is worth noting that the behavior of the local Kondo scales and the density of states are in agreement with the previous works as in Refs. 29 and 31. In our work we perform a detailed investigation of the spectra, and find that the broad distribution of Kondo scales and the underlying universal scattering dynamics corroborate the physical picture of the emergence of the formation of local moments in the presence of metallic droplets, as proposed in Refs. 31 and 55. While the emergent local moments would tend towards a common Kondo scale, we speculate that the Kondo scales and hence the low energy physics associated with the metallic droplets could be inhomogeneous. These observations are particularly relevant for understanding the underlying mechanisms that lead to the breakdown of the metallic phase towards a Mott or Mott-Anderson localization transition. However, in order to assert the true nature of this spatial inhomogeneity we require to go beyond the local framework and incorporate non-local dynamical fluctuations.

The local moment approach is an inherently non-perturbative impurity solver neither confined to low energies like the slave-boson approach nor to weak coupling like the iterated perturbation theory or modified perturbation theory approaches. While for non-disordered correlated systems this has clearly been demonstrated^{50,56}, our present calculations show that it does capture the strong correlation physics in accordance with the numerically exact NRG calculations for disordered correlated systems²⁹. With this set up established, one then asks the question as to what happens if we include short-range dynamical fluctuations due to disorder. Such directions within the framework of the typical medium dynamical cluster approximation⁵⁷ are currently under our consideration.

ACKNOWLEDGMENTS

We would like to acknowledge fruitful discussions with Pinaki Majumdar and Subroto Mukerjee. S.S. acknowledges the financial support from CSIR, India and JN-CASR, India. This material is based upon work supported by the National Science Foundation award DMR-1237565 and by the EPSCoR Cooperative Agreement EPS-1003897 with additional support from the Louisiana Board of Regents. Supercomputer support is provided by the Louisiana Optical Network Initiative (LONI) and HPC@LSU.

Appendix A: Local moment approach (LMA)

1. Starting point: unrestricted Hartree Fock

In the following we will discuss some of the basic concepts of the zero temperature LMA formalism. A key physical aspect of this method is the inclusion of low energy spin-flip excitations in the single-particle dynamics. This is facilitated at the inception by starting from the unrestricted Hartree Fock (UHF) state: local moments, $\bar{\mu}$, are introduced from the outset, to get a direct handle on the low energy spin-flip processes. The solutions are built around simple symmetry broken static mean-field, UHF, states, containing two degenerate states $\bar{\mu} = \pm|\bar{\mu}|$, where, $|\bar{\mu}| = |\langle \hat{n}_{i\uparrow} - \hat{n}_{i\downarrow} \rangle|$, the average being over the UHF ground state. We label A and B for solutions $\bar{\mu} = +|\bar{\mu}|$ or $-|\bar{\mu}|$ respectively⁵⁰. For an understanding of the formal details the reader is referred to^{16,38,42,50,58,59}. Here, we briefly recap the main equations. The single particle UHF Green's functions for the paramagnetic case, are given by,

$$\mathcal{G}_{\uparrow}^{UHF}(\omega) = \frac{1}{\omega^+ - e_i + x - \Gamma(\omega)}, \quad (\text{A1})$$

$$\mathcal{G}_{\downarrow}^{UHF}(\omega) = \frac{1}{\omega^+ - e_i - x - \Gamma(\omega)}, \quad (\text{A2})$$

where, $\Gamma(\omega)$ is the hybridization function for the impurity-host coupling, that, for the paramagnetic case, is spin independent; $x = \frac{1}{2}|\bar{\mu}|U$ and $e_i = \epsilon_i + \frac{1}{2}Un$, where n is the mean-field charge as described in the following. The density of the single-particle excitations is given by, $\mathcal{D}_{\sigma} = -\frac{1}{\pi}\text{Im}\mathcal{G}_{\sigma}^{UHF}(\omega)$, where, $\sigma = \uparrow / \downarrow$. The local moment, in general, would be given by, $|\bar{\mu}| = \int_{-\infty}^0 d\omega (\mathcal{D}_{\uparrow}(\omega) - \mathcal{D}_{\downarrow}(\omega))$, and has to be obtained *self-consistently*. When we are away from particle-hole symmetry then we also need the impurity occupancy to be given by, $\tilde{n} = \int_{-\infty}^0 d\omega (\mathcal{D}_{\uparrow}(\omega) + \mathcal{D}_{\downarrow}(\omega))$. For the pure mean-field UHF solution, we have,

$$\tilde{\mu} = \bar{\mu} \quad (\text{A3})$$

$$\tilde{n} = n, \quad (\text{A4})$$

to be solved self-consistently. So, if we now fix x and e_i (note that they are not the bare parameters of the Hamiltonian), then Eqs. (A3) and (A4) would provide the solution at one shot and accordingly, the bare parameters may be inferred as $U = 2x/|\bar{\mu}|$ and $\epsilon_i = e_i - Un/2$. However, if U and ϵ_i are fixed then this has to be obtained by iterative cycling. The UHF solution is severely deficient (see^{42,50,58,60,61}), for not capturing the Fermi liquid picture. In any case, being a static approximation, one has to go beyond it to incorporate dynamics.

2. Inclusion of spin-flip scattering dynamics

Within the LMA in practice, we approximate the dynamical part of the self-energy by the (nonperturbative) class of spin-flip diagrams shown in Fig. 9. Here, the bare propagators are that of UHF and therefore the inclusion of all these diagrams constitute the UHF+random phase approximation (RPA) scheme. We thus build a two self-energy description, as represented in Fig. 9 and mathematically represented as,

$$\Sigma_{\sigma}(\omega) = U^2 \int_{-\infty}^{\infty} \frac{d\omega'}{2\pi i} \mathcal{G}_{\bar{\sigma}}^{UHF}(\omega - \omega') \Pi^{\bar{\sigma}\sigma}(\omega'). \quad (\text{A5})$$

$\Pi^{\bar{\sigma}\sigma}(\omega)$ is the transverse-spin polarization propagator (with $\bar{\sigma} = -\sigma$), which in the current RPA scheme employed is expressed as, $\Pi^{\bar{\sigma}\sigma}(\omega) = \frac{0\Pi^{\bar{\sigma}\sigma}}{1 - U^0\Pi^{\bar{\sigma}\sigma}}$. The bare polarization propagator, $0\Pi^{\bar{\sigma}\sigma}(\omega)$ is expressed in terms of broken symmetry mean-field propagators as, $0\Pi^{\bar{\sigma}\sigma}(\omega) = \frac{i}{2\pi} \int_{-\infty}^{\infty} d\omega' \mathcal{G}_{\downarrow}^{UHF}(\omega') \mathcal{G}_{\uparrow}^{UHF}(\omega' - \omega)$.

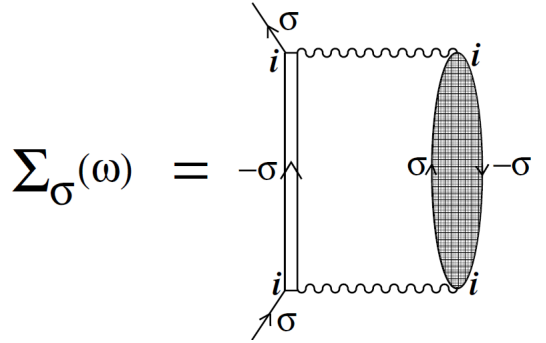


FIG. 9. **Self-energy within the LMA for the single impurity Anderson model:** Diagrammatic representation of the dynamic self-energy, $\Sigma(\omega)$ retained within the LMA in practice. The diagrams are expressed in terms of the polarization bubble, $\Pi^{\bar{\sigma}\sigma}(\omega)$. Wavy line: interaction, U , double line: renormalized host/medium propagator, hatched region: transverse spin polarization propagator bubble. See Eq. (A5) and the associated text.

The UHF propagators should result in a self-energy that satisfies the basic criteria for a Fermi liquid. After some detailed algebra⁵⁰, we can then arrive at self-consistency equation for determining the exact local mo-

ment that satisfies such constraints, so that the two self-energy description may be written as,

$$\sum_{\sigma} \sigma \Sigma_{\sigma}(0; e_i, x) = |\tilde{\mu}(e_i, x)|U. \quad (\text{A6})$$

The above equation is known as the symmetry-restoration condition. Finally, the single self-energy may be obtained as,

$$\Sigma(\omega) = \frac{1}{2} \left[\tilde{\Sigma}_{\uparrow}(\omega) + \tilde{\Sigma}_{\downarrow}(\omega) \right] + \frac{\frac{1}{2} \left(\tilde{\Sigma}_{\uparrow}(\omega) - \tilde{\Sigma}_{\downarrow}(\omega) \right)^2}{g^{-1}(\omega) - \frac{1}{2} \left[\tilde{\Sigma}_{\uparrow}(\omega) + \tilde{\Sigma}_{\downarrow}(\omega) \right]}, \quad (\text{A7})$$

where,

$$\tilde{\Sigma}_{\sigma}(\omega) = \frac{U}{2} (\tilde{n} - \sigma |\tilde{\mu}|) + \Sigma_{\sigma}(\omega), \quad (\text{A8})$$

with $\sigma = \uparrow / \downarrow$ and the impurity Green's function, $G_{imp} = \frac{1}{2} \sum_{\sigma} G_{\sigma}$, with $G_{\sigma}(\omega) = \left[g^{-1}(\omega) - \tilde{\Sigma}_{\sigma}(\omega) \right]^{-1}$ and $g(\omega) = \frac{1}{\omega + -\epsilon_i - \Gamma(\omega)}$. Additionally, for p-h asymmetric situations⁶⁰ one also needs to satisfy the Luttinger's theorem given by,

$$I_L = \text{Im} \int_{-\infty}^0 \frac{d\omega}{\pi} \frac{\partial \Sigma(\omega)}{\partial \omega} G_{imp}(\omega) = 0. \quad (\text{A9})$$

The self-consistent imposition of Eq. (A6) amounts to a self-consistency condition for the local moment $|\tilde{\mu}|$ that enters Eqs. (A1), (A2). A low energy spin-flip scale, T_K is generated; this scale that manifests as a strong resonance in the imaginary part of the transverse spin polarization propagator, $\text{Im} \Pi^{\sigma\sigma}(\omega)$, is proportional to the Kondo scale^{50,60}. If the symmetry-restoration condition Eq (A6) is not satisfied then a spin-flip scale occurs at $T_K = 0$ signaling the breakdown of a Fermi liquid.

A practical implementation of the LMA involves fixing $x = \frac{1}{2}U|\tilde{\mu}|$ and e_i ^{16,42,43,50,58,62}. The current nature of the problem, however, requires us to fix the bare parameters of the single impurity Anderson model, namely, U and ϵ_i . However, we should also note that if ϵ_i is fixed instead of e_i then, Eq. (A6) and Eq. (A9) would have to be solved self-consistently requiring several $\sim 20 - 30$ symmetry-restoration steps increasing the computation time enormously. Instead, if we fix U and e_i and tune $\tilde{\mu}$ we can drastically reduce this requirement again ending up in solving 5-6 symmetry-restoration iterations, as in the fixed x , fixed e_i algorithm. The scheme is described as following:

1. We start with an initial guess local moment, $\tilde{\mu}$ with which we calculate $\mathcal{G}_{\uparrow/\downarrow}$ and subsequently, $\tilde{\mu}$ from UHF spectral functions.
2. The calculation of ${}^0\Pi^{\sigma\sigma}$ and $\Pi^{\sigma\sigma}$, and, $\Sigma_{\uparrow/\downarrow}$ follows.

3. Eq. (A6) is checked and steps (1), (2), (3) are repeated until a convergence of 10^{-6} or lower is achieved. With this step it can be realized that the entire process involves calculations of coupled equations for finding the root of Eq. (A6), for which one therefore has to provide a judicious guess to reach the solution correctly and efficiently.

4. Finally, with proper guesses for the underlying self-consistency equations a converged $\Sigma(\omega)$ is obtained. With this self-energy, we can now satisfy Eq. (A9) by tuning ϵ_i .

In particular to the problem treated in this paper, we also had to take care of the computation time required to be able to sample sufficient number of disorder realizations. We achieved this by bringing in some additional *schemes* which would be discussed in detail in the following section.

Appendix B: Numerical implementation of TMT-DMFT

In this section we provide technical details of our implementation of the LMA within the TMT-DMFT framework. For the sake of completeness we also outline the steps involved in the TMT-DMFT implementation. As outlined in the previous section, employing the LMA with the bare parameters U and ϵ_i , would require a lot of computational time. This results from the fact that, away from p-h symmetry the impurity parameter e_i that acts like a *pseudo chemical potential* and explicitly enters the UHF Green's functions via Eqs. (A1), (A2), would have to be tuned so that the symmetry-restoration (Eq. (A6)) and the Luttinger's theorem (Eq. (A9)) are self-consistently satisfied. Recall that this would result in repeating the symmetry restoration (Eq. (A6)) step described in several times. Instead, the impurity self-energy may be obtained at a much cheaper effort if the bare parameters U and the impurity parameter e_i is fixed. In that case, once the symmetry restored impurity self-energy and Green's functions are obtained, one can tune the ϵ_i such that the the Luttinger's theorem (Eq. (A9)) is satisfied. This can be done without having to repeat the impurity self-energy calculation. However, in the current problem, the ϵ_i is a random quantity following a particular distribution. So, in order to resort to the fixed U , fixed e_i scheme discussed in the earlier section we have to first build a *database* for the respective (e_i, ϵ_i) pair with the given hybridization. In other words, before going to the actual calculation we do the following:

Step 1:

1. Given a hybridization function, $\Gamma(\omega)$ we start from the particle-hole symmetric limit with $e_i = 0$ and $\epsilon_i = -U/2$, for which the Luttinger's theorem (Eq. (A9)) is naturally satisfied. Note that in the main text, $\Gamma(\omega)$, has been denoted as $\Gamma_{typ}(\omega)$. So,

in this step the LMA solver is provided with (a) $\Gamma(\omega)$, (b) U , (c) $e_i = 0$.

2. We now increment the e_i by a small step, say 0.02^{63} . So, in this step the LMA solver is provided with (a) $\Gamma(\omega)$, (b) U , (c) $e_i = 0.02$. Accordingly, the ϵ_i is derived by satisfying the Luttinger's theorem (Eq. (A9)) and an (e_i, ϵ_i) pair for the given $\Gamma(\omega)$ is generated.
3. The above step (2) is continued until the ϵ_i obtained overshoots the limit set by the disorder strength, W . Note that, $\epsilon_i = -U/2 + V_i$, where V_i is a random number between $-W \leq V_i \leq W$.
4. For the actual random configuration, V_i , and therefore, the ϵ_i , we now interpolate the corresponding e_i from the database and compute the local self-energy, Σ_i . Finally, we construct the local Green's function, $G_i(\omega, V_i)$, using the equation, $G_i(\omega, V_i) = ([\mathcal{G}]^{-1}(\omega) - \Sigma_i(\omega) - \epsilon_i)^{-1}$, where, $\mathcal{G}(\omega) = \frac{1}{\omega + \Gamma(\omega)}$. This would now be used to construct $\rho_{typ}(\omega)$.

Step 2:

The output of the **Step 1** comprises N local impurity self-energies, $\Sigma_i(\omega)$ that gives us N local impurity Green's function, $G_i(\omega)$. With the local spectral functions, $\rho_i(\omega) = -\frac{1}{\pi} \text{Im} G_i(\omega)$, we construct the disorder averaged DoS, using geometric averaging:

$$\rho_{typ}(\omega) = \exp \int dV_i P(V_i) \ln \rho_i(\omega) \quad (\text{B1})$$

Using Eq. (B1) we can now construct the *typical* Green's function, $G_{typ}(\omega)$, from the Hilbert transform of ρ_{typ} :

$$G_{typ}(\omega) = \int \frac{\rho_{typ}(\omega') d\omega'}{\omega - \omega'}. \quad (\text{B2})$$

Step 3: We define the coarse-grained lattice Green's function as $\overline{G}(\omega)$, given by,

$$\overline{G}(\omega) = \int \frac{\rho_0(\epsilon) d\epsilon}{[G_{typ}(\omega)]^{-1} + \Gamma(\omega) - \epsilon}, \quad (\text{B3})$$

where $\rho_0(\epsilon)$ refers to the bare density of states, that in the current problem is that of the 3-dimensional cubic lattice.

Step 4: The new hybridization may be obtained as,

$$\Gamma(\omega)_{new} = \Gamma_{old} + \zeta [(G_{typ})^{-1} - (\overline{G})^{-1}], \quad (\text{B4})$$

where, ζ is a mixing parameter typically set to a value of 0.5. With $\Gamma_{new}(\omega)$ we can go back to **Step 1** and continue until $-\text{Im} \int |(\Gamma_{new}(\omega) - \Gamma_{old}(\omega))| d\omega$ converges within some tolerance, which in our implementation is chosen to be $\sim 10^{-3}$.

Note that in order to look into the scattering dynamics, we calculate the arithmetic average of the local density of states, $\rho_i(\omega)$. As described in the main text, this is given by, $\rho_{arith} = \int dV_i P(V_i) \rho_i(\omega)$ and it represents the average density of states (ADoS) of the lattice. From the ADoS, we can then calculate the arithmetic average of the local Green's function, $\langle G(\omega) \rangle_{arith}$, using the, Hilbert transform relation, $\langle G(\omega) \rangle_{arith} = \int \frac{\rho_{arith}(\omega') d\omega'}{\omega - \omega'}$. The disorder-averaged self-energy, $\Sigma(\omega)$, that represents the scattering dynamics is then calculated as, $\Sigma_{ave}(\omega) = \mathcal{G}(\omega)^{-1} - \langle G(\omega) \rangle_{arith}^{-1}$.

REFERENCES

-
- * raja@jncasr.ac.in
 † jarrellphysics@gmail.com
- ¹ F. Evers and A. D. Mirlin, Rev. Mod. Phys. **80**, 1355 (2008).
 - ² B. Kramer and A. MacKinnon, Rev. Prog. Phys. **56**, 1469 (1993).
 - ³ E. Abrahams, *Fifty Years of Anderson Localization* (Singapore: World Scientific, 2010).
 - ⁴ G. Kotliar and D. Vollhardt, Physics Today **57**, 53 (2004).
 - ⁵ A. Georges, G. Kotliar, W. Krauth, and M. J. Rozenberg, Rev. Mod. Phys. **68**, 13 (1996).
 - ⁶ P. W. Anderson, Phys. Rev. **109**, 1492 (1958).
 - ⁷ S. V. Kravchenko and M. P. Sarachik, Reports on Progress in Physics **67**, 1 (2004).
 - ⁸ E. Miranda and V. Dobrosavljević, Reports on Progress in Physics **68**, 2337 (2005).
 - ⁹ K. Maiti, R. S. Singh, and V. R. R. Medicherla, Phys. Rev. B **76**, 165128 (2007).
 - ¹⁰ K. W. Kim, J. S. Lee, T. W. Noh, S. R. Lee, and K. Char, Phys. Rev. B **71**, 125104 (2005).
 - ¹¹ A. S. Sefat, J. E. Greedan, G. M. Luke, M. Niéwczas, J. D. Garrett, H. Dabkowska, and A. Dabkowski, Phys. Rev. B **74**, 104419 (2006).
 - ¹² L. Sanchez-Palencia and M. Lewenstein, Nature Physics **6**, 87 (2010).
 - ¹³ M. White, M. Pasienski, D. McKay, S. Q. Zhou, D. Ceperley, and B. DeMarco, Phys. Rev. Lett. **102**, 055301 (2009).
 - ¹⁴ S. S. Kondov, W. R. McGehee, W. Xu, and B. DeMarco, Phys. Rev. Lett. **114**, 083002 (2015).
 - ¹⁵ P. A. Lee and T. V. Ramakrishnan, Rev. Mod. Phys. **57**, 287 (1985).
 - ¹⁶ N. S. Vidhyadhiraja and D. E. Logan, European Physical Journal B **39**, 313 (2004).

- ¹⁷ Q. Si and F. Steglich, *Science* **329**, 1161 (2010).
- ¹⁸ R. Bulla and T. Pruschke, “Strong electronic correlations and low energy scales,” in *Open Problems in Strongly Correlated Electron Systems*, edited by J. Bonča, P. Prelovšek, A. Ramšak, and S. Sarkar (Springer Netherlands, Dordrecht, 2001) pp. 381–386.
- ¹⁹ D. E. Logan and M. R. Galpin, *Journal of Physics: Condensed Matter* **28**, 025601 (2016).
- ²⁰ M. M. Radonjić, D. Tanasković, V. Dobrosavljević, K. Haule, and G. Kotliar, *Phys. Rev. B* **85**, 085133 (2012).
- ²¹ S. V. Kravchenko and M. P. Sarachik, *Reports on Progress in Physics* **67**, 1 (2004).
- ²² B. Spivak, S. V. Kravchenko, S. A. Kivelson, and X. P. A. Gao, *Rev. Mod. Phys.* **82**, 1743 (2010).
- ²³ M. C. O. Aguiar, V. Dobrosavljević, E. Abrahams, and G. Kotliar, *Phys. Rev. B* **71**, 205115 (2005).
- ²⁴ B. Altshuler and A. Aronov, in *Electron-electron interactions in disordered systems*, edited by A.L. Efros and M. Pollak (North-Holland, Amsterdam, 1985).
- ²⁵ A. Punnoose and A. M. Finkel’stein, *Science* **310**, 289 (2005).
- ²⁶ A. Finkelstein, in *Soviet Science Reviews*, Vol. 9 (edited by I.M. Khalatnikov (Harwood Academic, London, 1990), 1990) p. 3.
- ²⁷ V. Dobrosavljević, A. A. Pastor, and B. K. Nikolić, *Europhysics Letters* **62**, 76 (2003).
- ²⁸ G. Schubert, J. Schleede, K. Byczuk, H. Fehske, and D. Vollhardt, *Phys. Rev. B* **81**, 155106 (2010).
- ²⁹ K. Byczuk, W. Hofstetter, and D. Vollhardt, *Phys. Rev. Lett.* **94**, 056404 (2005).
- ³⁰ M. C. O. Aguiar, V. Dobrosavljević, E. Abrahams, and G. Kotliar, *Phys. Rev. B* **73**, 115117 (2006).
- ³¹ M. C. O. Aguiar, V. Dobrosavljević, E. Abrahams, and G. Kotliar, *Phys. Rev. Lett.* **102**, 156402 (2009).
- ³² K. Byczuk, W. Hofstetter, and D. Vollhardt, in *50 years of Anderson localization*, edited by E. Abrahams (World Scientific, 2010) p. 473.
- ³³ M. C. O. Aguiar and V. Dobrosavljević, *Phys. Rev. Lett.* **110**, 066401 (2013).
- ³⁴ K. Byczuk, W. Hofstetter, U. Yu, and D. Vollhardt, *The European Physical Journal Special Topics* **180**, 135 (2009).
- ³⁵ V. Dobrosavljević, A. A. Pastor, and B. K. Nikolić, *Europhysics Letters* **62**, 76 (2003).
- ³⁶ D. Sénéchal, A.-M. Tremblay, and C. Bourbonnais, *Theoretical methods for strongly correlated electrons* (Springer Science & Business Media, 2006).
- ³⁷ A. Benlagra, T. Pruschke, and M. Vojta, *Phys. Rev. B* **84**, 195141 (2011).
- ³⁸ D. E. Logan, M. P. Eastwood, and M. A. Tusch, *Journal of Physics Condensed Matter* **10**, 2673 (1998).
- ³⁹ M. T. Glossop and D. E. Logan, *Journal of Physics: Condensed Matter* **15**, 7519 (2003).
- ⁴⁰ R. Bulla, M. T. Glossop, D. E. Logan, and T. Pruschke, *Journal of Physics: Condensed Matter* **12**, 4899 (2000).
- ⁴¹ D. E. Logan, M. P. Eastwood, and M. A. Tusch, *Journal of Physics Condensed Matter* **9**, 4211 (1997).
- ⁴² V. Smith, D. Logan, and H. Krishnamurthy, *The European Physical Journal B* **32**, 49 (2003).
- ⁴³ H. Barman, *Phys. Rev. B* **94**, 045106 (2016).
- ⁴⁴ J. Bonča, T. Pruschke, *et al.*, *Phys. Rev. B* **80**, 245112 (2009).
- ⁴⁵ B. R. Bulka, B. Kramer, and A. MacKinnon, *Zeitschrift für Physik B Condensed Matter* **60**, 13 (1985).
- ⁴⁶ B. Bulka, M. Schreiber, and B. Kramer, *Zeitschrift für Physik B Condensed Matter* **66**, 21 (1987).
- ⁴⁷ M. Milovanović, S. Sachdev, and R. N. Bhatt, *Phys. Rev. Lett.* **63**, 82 (1989).
- ⁴⁸ R. N. Bhatt and D. S. Fisher, *Phys. Rev. Lett.* **68**, 3072 (1992).
- ⁴⁹ X. Deng, J. Mravlje, M. Ferrero, G. Kotliar, A. Georges, *et al.*, *Phys. Rev. Lett.* **110**, 086401 (2013).
- ⁵⁰ D. E. Logan, M. P. Eastwood, and M. A. Tusch, *Journal of Physics: Condensed Matter* **10**, 2673 (1998).
- ⁵¹ E. C. Andrade, E. Miranda, and V. Dobrosavljević, *Phys. Rev. Lett.* **102**, 206403 (2009).
- ⁵² D. Tanasković, V. Dobrosavljević, E. Abrahams, and G. Kotliar, *Phys. Rev. Lett.* **91**, 066603 (2003).
- ⁵³ E. Andrade, E. Miranda, and V. Dobrosavljević, *Physica B: Condensed Matter* **404**, 3167 (2009), proceedings of the International Conference on Strongly Correlated Electron Systems.
- ⁵⁴ R. Žitko, D. Hansen, E. Perepelitsky, J. Mravlje, A. Georges, and B. S. Shastry, *Phys. Rev. B* **88**, 235132 (2013).
- ⁵⁵ M. A. Paalanen, J. E. Graebner, R. N. Bhatt, and S. Sachdev, *Phys. Rev. Lett.* **61**, 597 (1988).
- ⁵⁶ M. R. Galpin and D. E. Logan, *Journal of Physics: Condensed Matter* **17**, 6959 (2005).
- ⁵⁷ C. E. Ekuma, H. Terletska, K.-M. Tam, Z.-Y. Meng, J. Moreno, and M. Jarrell, *Phys. Rev. B* **89**, 081107 (2014).
- ⁵⁸ M. T. Glossop and D. E. Logan, *Journal of Physics: Condensed Matter* **14**, 6737 (2002).
- ⁵⁹ N. L. Dickens and D. E. Logan, *Journal of Physics Condensed Matter* **13**, 4505 (2001).
- ⁶⁰ M. T. Glossop and D. E. Logan, *Journal of Physics: Condensed Matter* **14**, 6737 (2002).
- ⁶¹ D. E. Logan and M. T. Glossop, *Journal of Physics: Condensed Matter* **12**, 985 (2000).
- ⁶² N. S. Vidhyadhiraja and D. E. Logan, *Journal of Physics: Condensed Matter* **17**, 2959 (2005).
- ⁶³ This is optimized by experience to minimize the number of steps or (e_i, ϵ_i) pairs required to obtain a *good* database.